

# Image classification using separable invariant moments of Charlier-Meixner and support vector machine

Abdeslam Hmimid<sup>1</sup> · Mhamed Sayyouri<sup>2</sup> ·  
Hassan Qjidaa<sup>1</sup>

Received: 30 May 2017 / Revised: 4 January 2018 / Accepted: 7 January 2018 /  
Published online: 1 February 2018  
© Springer Science+Business Media, LLC, part of Springer Nature 2018

**Abstract** In this paper, we propose a new method for image classification by the content in heterogeneous databases. This approach is based on the use of new series of separable discrete orthogonal moments as shape descriptors and the Support Vector Machine as classifier. In fact, the proposed descriptors moments are defined from the bivariate discrete orthogonal polynomials of Charlier-Meixner which are invariant to translation, scaling and rotation of the image. We also propose a new algorithm to accelerate the image classification process. This algorithm is based on two steps: the first step is the fast computation of the values of Charlier-Meixner polynomials by using a new recurrence relationship between the values of polynomials Charlier-Meixner. The second one is the new image representation and slice blocks. The proposed method is tested on three different sets of standard data which are well known to computer vision: COIL-100, 256-CALTECH and Corel. The simulation results show the invariance of the discrete orthogonal separable moments of Charlier-Meixner against the various geometric transformations and the ability for the classification of heterogeneous images.

**Keywords** Bivariate polynomials · Charlier-Meixner invariant moments · Pattern recognition, classification, support vector machine

---

✉ Mhamed Sayyouri  
mhamed.sayyouri@usmba.ac.ma

Abdeslam Hmimid  
abdeslam\_ph@yahoo.fr

Hassan Qjidaa  
qjidah@yahoo.fr

<sup>1</sup> CED-ST; LESSI, Faculty of Sciences Dhar El Mehraz, Sidi Mohamed Ben Abdellah University, BP 1796 Fez-Atlas, 30003 Fez, Morocco

<sup>2</sup> Laboratoire des Sciences de l'Ingénieur pour l'Energie (LapSIPE), Ecole Nationale des Sciences Appliquées d'El Jadida (ENSAJ), Université Chouaïb Doukkali, BP 1166, 24004 EL Jadida Plateau, Morocco

## 1 Introduction

The use of image moments constitutes one of the hotly debated issues in pattern recognition and image classification. The basic idea of the theory of moments is the projection of the data space on a complete orthogonal basis to often extract useful information. These latter are extracted as the projection coefficients called moments. Each family of moment is directly related to the basis of used projection. We can distinguish between three types of moments: the non-orthogonal moments as the geometric moments [16] and the complex moments [1], the continuous orthogonal moments as Legendre [47], Zernike [21], Pseudo-Zernike [48], Gegenbauer [15] and Fourier-Mellin [59] and the discrete orthogonal moments as Tchebichef [35], Krawtchouk [52], Racah [62], Charlier [12] and Hahn [43]. The computation of non-orthogonal moments and the continuous orthogonal moments requires appropriate transformations of the coordinates of the image in the interval of definition of the polynomials and also of the integrals by finite summations as well, because the function of the image intensity is always defined on a discrete domain. These approximations cause the discretization errors [25]. To definitely eliminate these errors, the researchers proposed using a discrete orthogonal moment based on the discrete orthogonal polynomials as the polynomials of Tchebitchef, Krawtchouk, Racah, Dual-Hahn, Hahn, Charlier and Meixner for image analysis. The use of this type of polynomials as basis functions for the computation of moments of the image eliminates the need for numerical approximation and satisfies exactly the orthogonality property in discrete space coordinates of the image. This property makes the discrete orthogonal moment higher than the conventional continuous orthogonal moment in terms of the capacity of the image representation. Recently, a novel set of discrete orthogonal moments based on the bivariate discrete orthogonal polynomials have been introduced into the field of the image analysis and pattern recognition [13, 49, 61]. These series of bivariate polynomials are solutions of the second-order partial differential Eqs [6, 8, 23]. The use of discrete orthogonal moments is limited by the high computational cost and the propagation of a numerical error in the computation of polynomials values [64]. To limit this error, the scientists apply the recurrence relation with respect to the variable  $x$  instead of the order  $n$  in the computation of the discrete orthogonal polynomials [64]. Thus, To reduce the computational time cost of moments, several algorithms are introduced in literature [9, 14, 37, 38, 40, 41, 45, 46].

Although most work has focused on the discrete moments based on the bivariate discrete orthogonal polynomials of Tchebichef-Krawtchouk [61], Tchebichef-Hahn [61], Hahn-Krawtchouk [61], Charlier-Tchebichef [12], Charlier-Krawtchouk [12] and Charlier-Hahn [12], no attention has been paid to the study of discrete orthogonal moments based on the bivariate discrete orthogonal polynomials of Charlier-Meixner.

In this paper, we will apply the discrete orthogonal moments for the classification problem of images in heterogeneous bases. The classification of image passes by the selection of the primitives, the latter is an important step in any pattern recognition system. This selection of primitives is considered a combinatorial optimization problem and has been researched in many disciplines. Its main purpose is to reduce their number by eliminating redundant and irrelevant primitives from the recognition system. The second objective of this selection of primitives is also to maintain and / or improve the performance of the classifier used by the recognition system. Invariant moments are used to solve this type of primitive selection problem in pattern recognition.

In this paper, we will present a new application of discrete orthogonal moments in the field of classification. This new method is applied to solve the problem of selecting a subset of primitives in a pattern recognition problem. The latter is based on the use of slice and block image representation to extract the primitives of each image from the blocks of each slice, it allows us to improve the classification result and speed up the process of pattern recognition without affecting the property of invariance. In our case, we use the discrete orthogonal moments based on the product of Charlier and Meixner discrete orthogonal polynomials which are denoted Charlier-Meixner moments (CMM). We also present an approach to accelerate the time computation of CMM based on two notions:

- The methodology of the image block representation (IBR) and the image slices representation (ISR): In this method the image is decomposed into series of non-overlapped binary slices and each slice is described by a number of homogenous rectangular blocks. Once the image is partitioned into slices and blocks, the computation of CMM can be accelerated as the moments can be computed from the blocks of each slice.
- The computation of the bivariate discrete orthogonal polynomials of Charlier-Meixner by using the recurrence relation with respect to the variable  $x$  instead of the order  $n$ .

We devote the rest of this paper to image classification systems by the content in heterogeneous databases. The images in this type basis belong to different concepts and are heterogeneous content. For this reason, we will test the ability of discrete orthogonal moments of Charlier-Meixner (CMM) for image classification in heterogeneous databases. For the purpose of objects classification, it is vital that the proposed moments of CMM is independent of rotation, scale and the translation of the image. For this, we have proposed a new set of discrete invariant moments of Charlier-Meixner (CMMI) under translation, scaling and rotation of the image. The invariant moments of Charlier-Meixner (CMMI) are derived algebraically from the geometric invariant moments.

The obtained results during the selection of the primitives made it possible to reduce the complexity of the classification. The number of primitives has been significantly reduced compared to all the primitives extracted from the pattern recognition system while maintaining the system recognition rate performance. A fast computational algorithm of CMMI is also presented using the image slice representation method. In fact, we tested the ability of classification of our descriptor CMMI compared to other descriptors of Hu invariant moments, Charlier invariant moments (CCMI) and Meixner invariant moments (MMMI) for the three databases COIL-100, CALTECH-256 and COREL using as classifier the support vector machines (SVM) for number of the classes between 3 to 35. We will also compare our classification method with classification methods based on Convolution Neural Network (CNN), on Histograms of Oriented Gradient (HOG) and on scalable invariant characteristic transformation (SIFT). So, the classification results show the efficiency of the CMMI in terms of classification accuracy of images compared to those of Hu, CCMI and MMMI.

Hence, The rest of the paper is organized as follows: In Section 2, we present the work related to our contribution. In Section 3, we present the bivariate discrete orthogonal polynomials of Charlier-Meixner. Section 4 presents the fast computation of Charlier-Meixner's discrete orthogonal moments. Section 5 focuses on the deriving of CMMI from the geometric moments by two methods. Section 6 provides some experimental results concerning the invariability, the objects classification by CMMI and the support vector machine. Section 7 concludes the work.

## 2 Related work

Several works have dealt with the theory of moments and their applications in the image domain, especially for image classification. In this context, one quotes the works of Hu [16] which extracted seven invariant primitives of the geometric moments. Chong et al. [3, 4] have introduced an effective method to construct the translation and scale invariants of Legendre and Zernike moment. Zhu et al. [63] have proposed a method directly based on Tchebichef polynomials to make the translation and scale invariants of Tchebichef moments. Karakasis et al. [20] have proposed a generalized expression of the weighted dual Hahn moment invariants up to any order and for any value of their parameters based on a linear combination of geometric moments. Beyond what orthogonal moments can bring to the different fields of imagery, these can be exploited in combination with machine learning methods in other areas of research, such as recognition actions based on collected data [27–30], or the prediction of your career from your data on social networks [31, 39, 54], and many other possibilities of use, the discrete orthogonal moments are well suited for decision support.

The application of moment theory in the image domain is limited by the computational time cost of moments. To solve this problem, Spiliotis and Mertzios [46] have presented a fast algorithm to calculate the geometric moments for binary images using the image block representation (IBR). Hosny [14] has given a fast algorithm to calculate the geometric moments for gray-scale images using the image slice representation. Lim et al. [26] have presented a fast computation technique to calculate exactly Zernike moments by using cascaded digital filter outputs, without the need to compute geometric moments.

Shu et al. [45] introduced an approach to accelerate the time computation of Tchebichef moments by deriving some properties of Tchebichef polynomials. Sayyouri et al. have proposed in [41] and [42] a fast method to accelerate time computation of Charlier and Hahn moments using the image bloc representation.

For the learning problem, several works have dealt with this subject. In this context, Zechao et al. in [58] propose a novel data representation learning algorithm by jointly exploiting image understanding, feature learning and feature correlation. They also proposed a deep metric learning method by exploiting the heterogeneous data structure of community-contributed images [56, 57].

Inspired by the statistical theory of learning, the SVM support vector classifier is a binary classification method for supervised learning. Originally, SVM relies on the existence of a linear classifier that separates two classes into an appropriate space. Its extension to multi-class problems is quickly highlighted. [2, 19] In addition, to allow optimal separation in non-linearly separable cases, SVMs have proven that the use of multiple kernels generates more flexibility and improves the interoperability of these methods [24]. Given its performance, this classification method has become in a short period a standard tool in the state of the art for several recognition problems, in particular heterogeneous images by the content. Within this framework, Hu et al. in [17, 18, 53, 55, 60] propose the use of the support vector machine to classify defects in steel strip surface images, to effectively recognize aerial photographs and for categorization of fine-grained images by hierarchically locating discriminating object parts in each image. Other works [32, 33] are focused on the recognition of semantic involvement and the relationship between medical and medical conditions.

Recently a new series of discrete orthogonal moments is introduced by several researchers to improve the quality of image processing either for reconstruction or for classification. Dunkl and Xu in [6] have proposed an excellent paper of bivariate discrete orthogonal polynomials as

a product of two families of classical discrete orthogonal polynomials with one variable. Zhu has studied in [61] seven types of the continuous and discrete orthogonal moments based on the tensor product of two different orthogonal polynomials with one variable. Hmimid et al. have proposed in [12] a new set of bivariate discrete orthogonal polynomials, which are the product of Charlier’s discrete orthogonal polynomials with one variable by Tchebichef, Krawtchouk, and Hahn discrete orthogonal polynomials with one variable.

### 3 The bivariate discrete orthogonal polynomials

In this section, we present the definition and the basic properties of classical discrete orthogonal polynomials of two variables of Charlier-Meixner [7, 51]. The discrete orthogonal polynomials with two variables satisfy the following second partial order difference equation.

$$A_{1,1}(x, y)\Delta_1 \nabla_1 P_n(x, y) + A_{1,2}(x, y)\Delta_1 \nabla_2 P_n(x, y) + A_{2,1}(x, y)\Delta_2 \nabla_1 P_n(x, y) + A_{2,2}(x, y)\Delta_2 \nabla_2 P_n(x, y) + B_1(x, y)\Delta_1 P_n(x, y) + B_2(x, y)\Delta_2 P_n(x, y) = \lambda P_n(x, y) \tag{1}$$

where  $A_{i,j}$  and  $B_j$  for  $i, j = 1, 2$  are polynomials and  $\lambda$  is a real number.

The forward and the backward partial difference operators  $\Delta_i$  and  $\nabla_i$  for  $i = 1, 2$  are defined by

$$\begin{aligned} \Delta_1 u(x, y) &= u(x + 1, y) - u(x, y) & \Delta_2 u(x, y) &= u(x, y + 1) - u(x, y) \\ \nabla_1 u(x, y) &= u(x, y) - u(x - 1, y) & \nabla_2 u(x, y) &= u(x, y) - u(x, y - 1) \end{aligned} \tag{2}$$

The bivariate discrete orthogonal polynomials are constructed from the product of the classical discrete orthogonal polynomials with one variable [7]. Using this method, we can produce the bivariate discrete orthogonal polynomials of Charlier-Meixner.

#### 3.1 Bivariate discrete orthogonal polynomials of Charlier-Meixner

The bivariate discrete orthogonal of Charlier-Meixner are defined as the product of the Charlier and Meixner discrete orthogonal polynomials with one variable as follows [51]:

$$CM_{n,m}(x, y, a_1, \beta, \mu) = C_n^{a_1}(x) \times M_n^{(\beta, \mu)}(y) ; n \geq 0 ; m \geq 0 \tag{3}$$

where  $C_n^{a_1}(x)$  is the  $n^{th}$  discrete orthogonal polynomials of Charlier and  $M_n^{(\beta, \mu)}(x)$  is the  $n^{th}$  discrete orthogonal polynomials of Meixner.

The bivariate discrete orthogonal of Charlier-Meixner are orthogonal on the set  $V = \{(i, j) : i \in \mathbb{N}, j \in \mathbb{N}\}$  with respect to the weight function of the Charlier-Meixner discrete orthogonal polynomials  $w_{C, M}(x, y)$ :

$$w_{C, M}(x, y) = w_C(x) \times w_M(y) \tag{4}$$

where  $w_C(x)$  is weight function of Charlier and  $w_M(x)$  is weight function of Meixner.

The bivariate discrete orthogonal polynomials of Charlier-Meixner  $CM_{n, m}(x, y, a_1, \beta, \mu)$  satisfy the following linear partial difference equation:

$$x\Delta_1 \nabla_1 u(x, y) - \frac{1}{\mu - 1} y \Delta_2 \nabla_2 u(x, y) + [a_1 - x] \Delta_1 u(x, y) - \frac{1}{\mu - 1} [\mu(y + \beta) - y] \Delta_2 u(x, y) - nu(x, y) = 0 \tag{5}$$

where  $u(x, y) = CM_{n, m}(x, y, a_1, \beta, \mu)$ .

In the next section, we will present a brief introduction to the theoretical background of discrete orthogonal polynomials with one variable of Charlier and Meixner [22, 36].

### 3.2 Discrete orthogonal polynomials with one variable of Charlier and Meixner

The discrete orthogonal polynomials with one variable of Charlier  $C_n^{a_1}(x)$  and Meixner  $M_n^{(\beta,\mu)}(x)$  satisfy the following first-order partial difference Eq. [31].

$$\sigma(x)\Delta\nabla P_n(x) + \tau(x)P_n(x) + \lambda_n P_n(x) = 0 \tag{6}$$

Where  $\sigma(x)$  and  $\tau(x)$  are the functions of second and first degree (Table 1), respectively,  $\lambda_n$  is an appropriate constant.

The  $n^{th}$  discrete orthogonal polynomials with one variable of Charlier  $C_n^{a_1}(x)$  and Meixner  $M_n^{(\beta,\mu)}(x)$  are defined by using a hypergeometric function as follows [63]:

$$C_n^{a_1}(x) = {}_2F_0(-n, -x; 1/a_1) = \sum_{k=0}^n \varepsilon_{k,n}^{a_1} x^k \tag{7}$$

where  $x, n = 0, 1, 2, \dots, N-1$  ;  $a_1 > 0$

$$M_n^{(\beta,\mu)}(x) = (\beta)_{n2} F_1(-n, -x; \beta; 1-1/\mu) = \sum_{k=0}^n \alpha_{k,n}^{(\beta,\mu)} x^k \tag{8}$$

where  $x, n = 0, 1, 2, \dots, N-1$ ;  $\beta > 0$  and  $0 < \mu < 1$ .

The set of Charlier's  $\{C_n^{a_1}(x)\}$ , Meixner's  $\{M_n^{(\beta,\mu)}(x)\}$  discrete orthogonal polynomials forms and a complete set of discrete basis functions with weight function satisfy the orthogonal condition:

$$\sum_{x=0}^N w(x)P_n(x)P_m(x) = \rho(n)\delta_{nm} \tag{9}$$

with  $P_n(x) = C_n^{a_1}(x)$  or  $M_n^{(\beta,\mu)}(x)$ .

where  $\rho(n)$  denotes the square of the norm of the corresponding orthogonal polynomials,  $w(x)$  denotes the weight function and  $\delta_{nm}$  denotes the Dirac function.

**Table 1** Data for Charlier  $C_n^{a_1}(x)$  and Meixner  $M_n^{(\beta,\mu)}(x)$

$\tilde{P}_n(x)$	Charlier $C_n^{a_1}(x)$	Meixner $M_n^{(\beta,\mu)}(x)$
$\sigma(x)$	$x$	$x$
$\tau(x)$	$a_1 - x$	$\beta\mu - x(1 - \mu)$
$\lambda_n$	$n$	$n(1 - \mu)$
$w(x)$	$\frac{e^{-a_1} a_1^n}{x!}$	$\frac{\mu^n \Gamma(\beta+x)}{\Gamma(\beta)x!}$
$\rho(n)$	$\frac{n!}{a_1^n}$	$\frac{n!(\beta)_n}{\mu^n (1-\mu)^n}$
$A$	$-a_1$	$\frac{\mu}{\mu-1}$
$B$	$x - n + 1 - a_1$	$\frac{x-x\mu-n+1-\mu n+\mu-\beta\mu}{1-\mu}$
$C$	$n - 1$	$\frac{(n-1)(n-2+\beta)}{1-\mu}$
$D$	$\sqrt{\frac{a_1}{n}}$	$\sqrt{\frac{\mu}{n(\beta+n-1)}}$
$E$	$\sqrt{\frac{a_1^2}{n(n-1)}}$	$\sqrt{\frac{\mu^2}{n(n-1)(\beta+n-2)}} \times \sqrt{\frac{\mu^2}{n(n-1)(\beta+n-2)}}$

To avoid fluctuations in the numerical computation of Charlier and Meixner discrete orthogonal polynomials, we use their normalized form defined as:

$$\tilde{P}_n(x) = P_n(x) \sqrt{\frac{w(x)}{\rho(n)}} \tag{10}$$

The computation of the values of polynomials of Charlier and Meixner, and from their definitions hypergeometric, requires a high cost of computing time which drives us to use a different strategy of computation which is the recursive strategy.

### 3.2.1 Recurrence relation with respect to order $n$

As the computation of the normalized form of Charlier and Meixner polynomials by the hypergeometric function has a great computational time cost, we use the following three-term recurrence relations with respect to the order  $n$  [22]:

$$\tilde{P}_n(x) = \frac{B \times D}{A} \tilde{P}_{n-1}(x) - \frac{C \times E}{A} \tilde{P}_{n-2}(x) \tag{11}$$

where A,B,C,D and E are the coefficient defined in Table 1.

The two initial values of Charlier’s and Meixner’s polynomials are defined as follows:

$$\tilde{C}_0^{a_1}(x) = \sqrt{\frac{w_C(x)}{\rho_C(0)}} \quad ; \quad \tilde{C}_1^{a_1}(x) = \frac{a_1 - x}{a_1} \sqrt{\frac{w_C(x)}{\rho_C(1)}} \tag{12}$$

and

$$\tilde{M}_0^{(\beta, \mu)}(x) = \sqrt{\frac{w_M(x)}{\rho_M(0)}} \quad ; \quad \tilde{M}_1^{(\beta, \mu)}(x) = \left( \beta + x - \frac{x}{\mu} \right) \sqrt{\frac{w_M(x)}{\rho_M(1)}} \tag{13}$$

### 3.2.2 Recurrence relation with respect to variable $x$

In order to extract the recurrence formula with respect to the variable  $x$  we will use the partial difference equations and the forward and backward finite difference operators. The recurrence relations of Charlier’s and Meixner’s discrete orthogonal polynomials with respect to the variable  $x$  can be obtained through Eqs. (2) and (6) as follows:

$$\begin{aligned} \tilde{p}_n(x) &= \frac{\sqrt{w(x)}}{\sigma(x-1) + \tau(x-1)} \\ &\times \left[ \frac{2\sigma(x-1) + \tau(x-1) - \lambda_n}{\sqrt{w(x-1)}} \tilde{p}_n(x-1) - \frac{\sigma(x-1) + \tau(x-1)}{\sqrt{w(x-2)}} \tilde{p}_n(x-2) \right] \end{aligned} \tag{14}$$

The initial values of recurrence relation with respect to the variable  $x$  are defined as:

$$\tilde{C}_n^{a_1}(0) = \sqrt{\frac{w_c(0)}{\rho_c(n)}} \quad ; \quad \tilde{C}_n^{a_1}(1) = \frac{a_1 - n}{a_1} \sqrt{\frac{w_c(1)}{w_c(0)}} \tilde{C}_n^{a_1}(0) \tag{15}$$

and

$$\tilde{M}_n^{(\beta, \mu)}(0) = (\beta)_n \sqrt{\frac{w_M(0)}{\rho_M(n)}} ; \quad \tilde{M}_n^{(\beta, \mu)}(1) = \frac{\mu(n + \beta) - n}{\mu\beta} \sqrt{\frac{w_M(1)}{w_M(0)}} M_n^{(\beta, \mu)}(0) \quad (16)$$

#### 4 Discrete orthogonal moments of Charlier-Meixner

The two-dimensional (2-D) discrete orthogonal moments of Charlier-Meixner (CMM) of order  $(n + m)$  for an image intensity function  $f(x, y)$  with size  $M \times N$  are defined as

$$CMM_{nm} = \sum_{x=0}^{M-1} \sum_{y=0}^{N-1} CM_{nm}(x, y, a_1, \beta, \mu) f(x, y) \quad (17)$$

where  $CM_{nm}(x, y, \beta, \mu, a_1)$  are the bivariate discrete orthogonal polynomials used as the moment basis set.

Using the orthogonal property of discrete orthogonal polynomials, Eq.(17) also leads to the following inverse moment transform:

$$f(x, y) = \sum_{n=0}^{M-1} \sum_{m=0}^{N-1} CMM_{nm} CM_{nm}(x, y, a_1, \beta, \mu) \quad (18)$$

The computation of Charlier-Meixner discrete orthogonal moments using Eq.(17) seems to be a time consuming task mainly due to two factors. First, the need of computing a set of complicated quantities for each moment order. Second, the need to evaluate the polynomial values for each pixel of the image. So, to accelerate the time computation of discrete orthogonal moments, we propose a new computation method of moments by describing an image with a set of blocks instead of individual pixels. Two algorithms of the image block representation: IBR for binary images [12, 43] and ISR for gray-scale images are applied. [13]

In the following two subsections, we will present a new formula for fast computing the discrete orthogonal moments of Charlier-Meixner by using the image block representation for binary and the image slice representation for gray-scale images.

##### 4.1 For gray-scale images

The approach of the image slice representation (ISR) decomposes a gray-scale image  $f(x, y)$  in series of slices of two levels  $f_i(x, y)$

$$f(x, y) = \sum_{i=1}^L f_i(x, y) \quad (19)$$

where  $L$  is the number of slices and  $f_i(x, y)$  the intensity function of the  $i^{th}$  slice. After the decomposition of the gray scale image into several slices of two levels, we can apply the algorithm IBR [46]. The gray-scale image  $f_i(x, y)$  can be redefined in terms of blocks of different intensities as follows:

$$f(x, y) = \{f_i(x, y), i = 1, 2, \dots, L\} = \{b_{ij}, j = 1, 2, \dots, K_i - 1\} \quad (20)$$

where  $b_{ij}$  is the block of the edge  $i$  and  $K_i$  is the number of image blocks with intensity.



The fast discrete orthogonal moments of Charlier-Meixner for a gray-scale image  $f(x, y)$  is given by:

$$\begin{aligned}
 CMM_{nm} &= \sum_{x=0}^{N-1} \sum_{y=0}^{N-1} CM_{nm}(x, y, a_1, \beta, \mu) f(x, y) \\
 &= \sum_{x=0}^{N-1} \sum_{y=0}^{N-1} \tilde{C}_n^{a_1}(x) \tilde{M}_m^{(\beta, \mu)}(y) \sum_{i=1}^L f_i(x, y) \\
 &= \sum_{i=1}^L \sum_{x=0}^{N-1} \sum_{y=0}^{N-1} \tilde{C}_n^{a_1}(x) \tilde{M}_m^{(\beta, \mu)}(y) f_i(x, y) \tag{21} \\
 &= \sum_{i=1}^L f_i \sum_{x=0}^{N-1} \tilde{C}_n^{a_1}(x) \sum_{y=0}^{N-1} \tilde{M}_m^{(\beta, \mu)}(y) \\
 &= \sum_{i=1}^L f_i \sum_{j=0}^{K_i-1} \left[ \sum_{x=x_{1,b_j}}^{x=x_{1,b_{j+1}}} \tilde{C}_n^{a_1}(x) \right] \left[ \sum_{y=y_{1,b_j}}^{y=y_{1,b_{j+1}}} \tilde{M}_m^{(\beta, \mu)}(y) \right]
 \end{aligned}$$

Note that, the binary images are particular cases of gray-scale images for  $L = 1$ .

### 5 Invariant moments of Charlier-Meixner

To use the Charlier-Meixner’s moments for the objects classification, it is indispensable that these moments must be invariant under rotation, scaling, and translation of the image. Therefore to obtain the translation, scale and rotation invariants moments of Charlier-Meixner (CMMI), we adopt the same strategy used by Sayyouri et al., for Hahn’s moments in [43]. Thus, we derive the CMMI through the geometric moments using the direct and the fast method based on the image slice representation methods.

#### 5.1 Geometric invariant moments

For a digital image  $f(x, y)$  with size  $M \times N$ , the geometric moments  $GM_{nm}$  are defined using discrete sum approximation as:

$$GM_{nm} = \sum_{x=0}^{N-1} \sum_{y=0}^{N-1} x^n y^m f(x, y) \tag{22}$$

The set of geometric invariant moments (GMI) by rotation, scaling and translation can be written as [16]:

$$GMI_{nm} = GM_{00}^{-\gamma} \sum_{x=0}^{N-1} \sum_{y=0}^{N-1} \left[ (x-\bar{x}) \cos \theta + (y-\bar{y}) \sin \theta \right]^n \left[ (y-\bar{y}) \cos \theta - (x-\bar{x}) \sin \theta \right]^m \tag{23}$$

with

$$\bar{x} = \frac{MG_{10}}{MG_{00}}; \bar{y} = \frac{MG_{01}}{MG_{00}}; \gamma = \frac{n+m}{2} + 1; \theta = \frac{1}{2} \tan^{-1} \frac{2\mu_{11}}{\mu_{20} - \mu_{02}} \tag{24}$$

The  $(n + m)$  th central geometric moments is defined in [16] by:

$$\mu_{nm} = \sum_{x=0}^{N-1} \sum_{y=0}^{N-1} (x-\bar{x})^n (y-\bar{y})^m f(x, y) \tag{25}$$

### 5.2 Computation of Charlier-Meixner’s invariant moments

The Charlier-Meixner’s moments of  $f(x, y)$  can be written in terms of geometric moments as:

$$\begin{aligned}
 CMM_{nm} &= [\rho_c(n)\rho_M(m)]^{-1/2} \sum_{x=0}^{M-1} \sum_{y=0}^{N-1} c_n^{a_1}(x)M_m^{(\beta,\mu)}(y)f(x, y) \\
 &= [\rho_c(n)\rho_M(m)]^{-1/2} \sum_{i=0}^n \sum_{j=0}^m \varepsilon_{i,n}^{a_1} \alpha_{j,m}^{(\beta,\mu)} GM_{ij}
 \end{aligned}
 \tag{26}$$

where the  $n^{th}$  order of Charlier and Meixner discrete orthogonal polynomials are given by:

$$C_n^{a_1}(x) = \sum_{k=0}^n \varepsilon_{k,n}^{a_1} x^k \quad \text{and} \quad M_n^{(\beta,\mu)}(x) = \sum_{k=0}^n \alpha_{k,n}^{(\beta,\mu)} x^k
 \tag{27}$$

The Charlier-Meixner’s invariant moments (CMMI) can be expanded in terms of GMI Eq. (23) as follows:

$$CMMI_{nm} = \sum_{i=0}^n \sum_{j=0}^m \varepsilon_{i,n}^{a_1} \alpha_{j,m}^{(\beta,\mu)} V_{i,j}
 \tag{28}$$

where  $\varepsilon_{i,n}^{a_1}$  and  $\alpha_{j,m}^{(\beta,\mu)}$  are the coefficients relative to Eq.(27) and  $V_{i,j}$  are the parameters defined as:

$$V_{nm} = \sum_{q=0}^n \sum_{p=0}^m \binom{n}{p} \binom{m}{q} \left(\frac{N \times M}{2}\right)^{((p+q)/2)+1} \times \left(\frac{N}{2}\right)^{n-p} \times \left(\frac{M}{2}\right)^{m-p} \times GMI_{pq}
 \tag{29}$$

### 5.3 Fast computation of Charlier-Meixner’s invariant moments

In order to accelerate the time computation of CMMI, we will apply the algorithms of the image slice representation described previously.

By using the binomial theorem, the GMI defined in Eq. (23) can be calculated as follows:

$$\begin{aligned}
 GMI_{nm} &= GM_{00}^{-\gamma} \sum_{i=0}^n \sum_{j=0}^m \binom{n}{i} \binom{m}{j} (\cos \theta)^{i+j} (\sin \theta)^{n+m-i-j} \times (-1)^{m-j} \mu_{m+i-j,n+j-i} \\
 &= \sum_{i=0}^n \sum_{j=0}^m \binom{n}{i} \binom{m}{j} (\cos \theta)^{i+j} (\sin \theta)^{n+m-i-j} \times (-1)^{m-j} \eta_{m+i-j,n+j-i}
 \end{aligned}
 \tag{30}$$

with  $\eta_{nm}$  are normalized central geometric moments defined as:

$$\eta_{nm} = \frac{\mu_{nm}}{GM_{00}^\gamma}
 \tag{31}$$

By applying the IBR algorithm, the normalized central moments defined in Eq. (31) can be calculated as follows:

$$\begin{aligned}
 \eta_{nm} &= \frac{\mu_{nm}}{GM_{00}^\gamma} = \frac{1}{GM_{00}^\gamma} \sum_{x=0}^{N-1} \sum_{y=0}^{M-1} (x-\bar{x})^n (y-\bar{y})^m f(x, y) \\
 &= \frac{1}{GM_{00}^\gamma} \sum_{x=0}^{N-1} \sum_{y=0}^{M-1} (x-\bar{x})^n (y-\bar{y})^m \left( \sum_{k=1}^S f_k(x, y) \right) \\
 &= \frac{1}{GM_{00}^\gamma} \sum_{k=1}^S f_k \times \sum_{x_k=0}^{N-1} \sum_{y_k=0}^{M-1} (x-\bar{x})^n (y-\bar{y})^m \tag{32} \\
 &= \frac{1}{GM_{00}^\gamma} \sum_{k=1}^S f_k \times \sum_{j=0}^k \left[ \left( \sum_{x_k=x_{1,b_j}}^{x_{2,b_j}} (x-\bar{x})^n \right) \left( \sum_{y_k=y_{1,b_j}}^{y_{2,b_j}} (y-\bar{y})^m \right) \right] \\
 &= \frac{1}{GM_{00}^\gamma} \sum_{k=1}^S f_k \times \eta_{nm}^k
 \end{aligned}$$

where

$$\eta_{nm}^k = \sum_{j=0}^k \left[ \left( \sum_{x_k=x_{1,b_j}}^{x_{2,b_j}} (x-\bar{x})^n \right) \left( \sum_{y_k=y_{1,b_j}}^{y_{2,b_j}} (y-\bar{y})^m \right) \right] \tag{33}$$

and  $f_k$  ;  $k = 1, 2, \dots, S$  is the slices intensity functions,  $S$  is the number of slices in image  $f$ .  $b_j$  ;  $j = 1, 2, \dots, k$  is the block in each slice. The vectors  $(x_{1,b_1}, y_{1,b_1})$  and  $(x_{2,b_1}, y_{2,b_1})$  are respectively the coordinates in the upper left and lower right block  $b_j$ .

Using the previous equations Eq.(31) and Eq.(33), the GMI of Eq.(30) can be rewritten as:

$$\begin{aligned}
 GMI_{nm} &= \sum_{i=0}^n \sum_{j=0}^m \binom{n}{i} \binom{m}{j} (\cos\theta)^{i+j} (\sin\theta)^{n+m-i-j} \times (-1)^{m-j} \eta_{m+i-j, n+j-i} \\
 &= \frac{1}{GM_{00}^\gamma} \sum_{i=0}^n \sum_{j=0}^m \binom{n}{i} \binom{m}{j} (\cos\theta)^{i+j} (\sin\theta)^{n+m-i-j} \times (-1)^{m-j} \sum_{k=1}^S f_k \times \eta_{m+i-j, n+j-i}^k \\
 &= \frac{1}{GM_{00}^\gamma} \sum_{k=1}^S f_k \sum_{i=0}^n \sum_{j=0}^m \binom{n}{i} \binom{m}{j} (\cos\theta)^{i+j} (\sin\theta)^{n+m-i-j} \times (-1)^{m-j} \times \eta_{m+i-j, n+j-i}^k \tag{34}
 \end{aligned}$$

Therefore the Charlier-Meixner invariant moments CMMI under translation, scaling and rotation of the image can be obtained from the equations Eqs. (28), (29) and (34).

### 6 Results and simulations

In this section, we give experimental results to validate the theoretical results developed in the previous sections. This section is divided into four subsections. In the first subsection, the invariability of the proposed discrete orthogonal moments of Charlier-Meixner under three transformations: translation, scale and rotation is shown. In the second, we test the precision of the classification of the CMMI invariant moments for four image databases. The results of our classification methods are compared to other moment descriptors for the classification of objects. In the third subsection, we will compare the proposed classification method with classification methods based on non-moment descriptors such as HOG, SIFT and CNN

features. In the fourth subsection, we will compare the calculation time of the Charlier-Meixner invariant moments by two methods: the direct method and the proposed fast method.

## 6.1 Invariability

In this section, we test the invariability of Charlier-Meixner invariant moments CMMI under the translation, the scale and the rotation of the image. For this, we will use a gray-scale image “Car” (Fig. 1) whose size is  $128 \times 128$  pixels chosen from the well-known Columbia database (<http://www.cs.columbia.edu/CAVE/databases>). This image is scaled by a factor varying from 0.5 to 1.5 with interval 0.05, rotated from  $0^0$  to  $360^0$  with interval  $10^0$  and translated by a vectors varying from  $(-5,-5)$  to  $(5,5)$ . Each translation vector consists of two elements which represent a vertical and a horizontal image shift respectively. All invariant moments of CMMI is calculated up to order two for each transformation. Finally, in order to measure the ability of the CMMI to remain unchanged under different image transformations, we define the relative error between the two sets of invariant moments corresponding to the original image  $f(x, y)$  and the transformed image  $g(x, y)$  as:

$$E_{CMM}(f, g) = \frac{\|CMMI(f) - CMMI(g)\|}{\|CMMI(f)\|} \quad (35)$$

where  $\|\cdot\|$  denotes the Euclidean norm and  $CMMI(f)$ ;  $CMMI(g)$  are invariant moments of Charlier-Meixner for the original image  $f$  and the transformed image  $g$ .

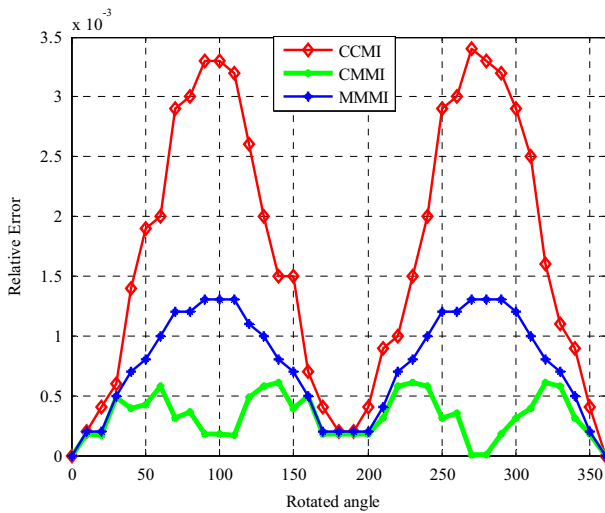
Figure 2 compares the relative errors between the proposed invariant moments of CMMI, the invariant moments of Meixner MMMI [44] and the invariant moments of Charlier CCMI [12] relative to rotation of the image. It can be seen from this figure that the CMMI is more stable under rotation (very low relative error) and has a better performance than the CCMI and MMMI whatever the rotational angle.

Figure 3 shows the relative errors between the CMMI, CCMI, and MMMI relative to scale. The figure shows that, in most cases, the relative error of CMMI is more stable and lower than the CCMI and MMMI.

Figure 4 shows the relative errors between the MMMI, CCMI, and CMMI relative to translation. The figure shows again that, in most cases, the relative error of CMMI is more stable

**Fig. 1** Car gray-scale image





**Fig. 2** Comparative study of relative errors between the rotated image and the original image by MMMi, CCMi and CMMi

and has a better performance than the CCMi and MMMi, whatever the translation vectors. Note that, the results are plotted in Figs. (2, 3 and 4) for the case  $a_1 = 80$  for the Charlier’s polynomials and  $\beta = 60$ ,  $\mu = 0.5$  for Meixner’s polynomials.

The results show that the CMMi is more stable under the translation, the scale and the rotation of the image than the CCMi, and MMMi.

To test the robustness to noise, we have respectively added a white Gaussian noise (with mean  $\mu = 0$  and different variances) and salt and pepper noise (with different noise densities). Results are respectively depicted in Figs. 5 and 6. It can be seen that, if the relative error increases with the noise level, the proposed descriptors of CMMi are more robust to noise than CCMi and MMMi.

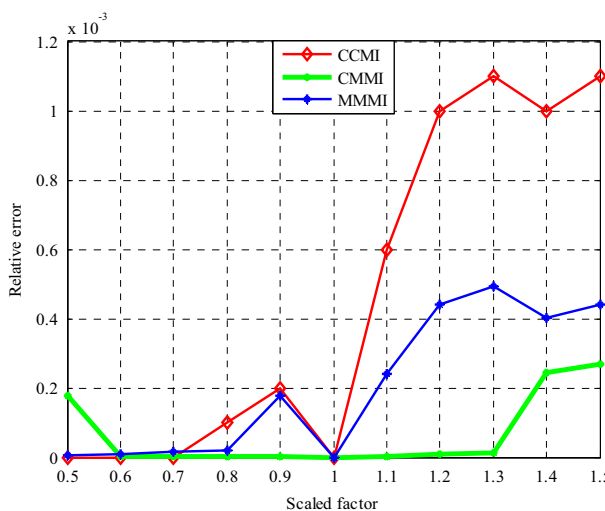


**Fig. 3** Comparative study of relative errors between the scaled image and the original image by MMMi, CCMi and CMMi

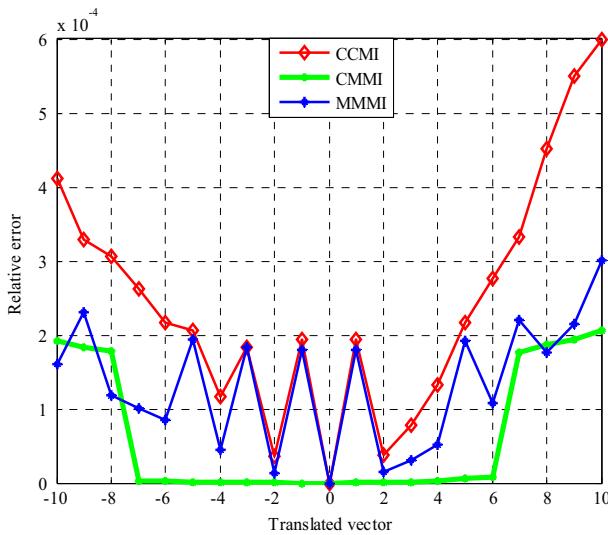


**Fig. 4** Comparative study of relative errors between the translated image and the original image by MMMI, CCMI and CMMI

### 6.2 Classification

In this section, we will provide experiments to validate the precision of the classification of objects using the CMMI. For this, we will put in place the characteristic vectors defined by:

$$V = [CMMI_{ij}]; i, j = 0, 1, 2 \tag{36}$$

To perform the classification of objects to their appropriate classes, we use classifiers based on support vector machines SVM.

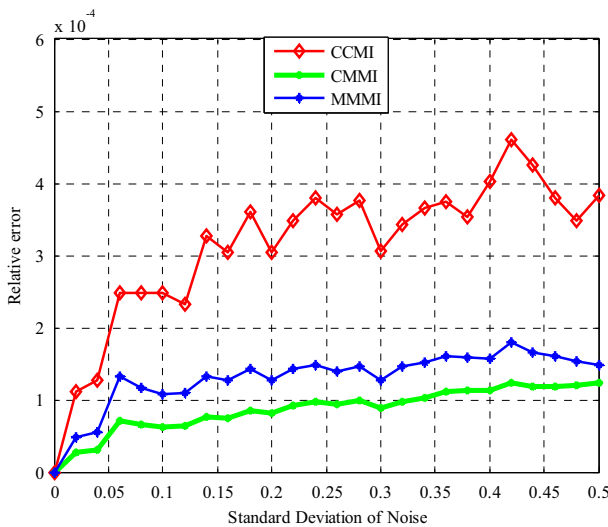


**Fig. 5** Comparative study of relative errors between the corrupted image (salt & pepper) and the original image by MMMI, CCMI and CMMI

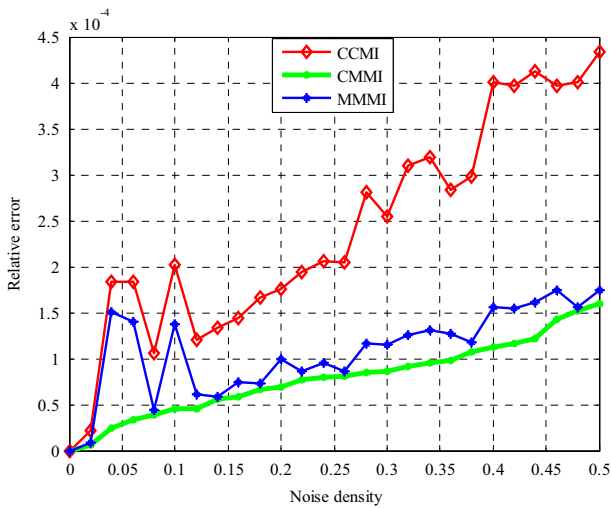


**Fig. 6** Comparative study of relative errors between the corrupted image (white Gaussian) and the original image by MMMI, CMI and CMMI

### 6.2.1 Classifier support vectors machines (SVM)

The classifier (SVM) was introduced by Vladimir Vapnik as a binary classification method for supervised learning [50]. This classification method has become in a short time a standard tool in the state of the art for several recognition problems. Initially, SVM relies on the existence of a linear classifier that separates two classes into an appropriate space. In addition, to allow optimal separation in non-linearly separable cases, SVMs have proven that the use of multiple nuclei generates more flexibility and improves the interoperability of these methods [11]. For two given classes of images, the goal of SVMs is to find a linear classifier that separates images while maximizing the distance between these two classes. This is a hyper-separation plan. The images closest to this hyper-plane, that is to say the most difficult to classify, are called support vectors. It is obvious that there is a multitude of valid hyper-planes but the remarkable property of the SVMs is that this hyper-plane must be optimal. Formally, this amounts to looking for a hyper-plane whose minimal distance to the different support vectors is maximal. There are two cases of SVM models: the linearly separable case and the non-linearly separable cases. The most used techniques for extending SVM to multi-class problems are based on “One- Against -One” or “One- Against -All” algorithms.

In our case, we will use the One-Against-All algorithm to implement the classification. And as descriptors, we use the invariant moments of Charlier-Meixner instead of using the images, we define the classification accuracy as:

$$\eta = \frac{\text{Number of correctly classified images}}{\text{The total of images used in the test}} \times 100\% \quad (37)$$

To validate the precision of the classification of objects using the CMMI, we will use three image databases. These databases are standard ones used by the scientific community during the testing and the validation of their approach and are freely available on the Internet. Each image database has defined the classes where each image belongs to one class. The first database is the Columbia Object Image Library (COIL-100) database





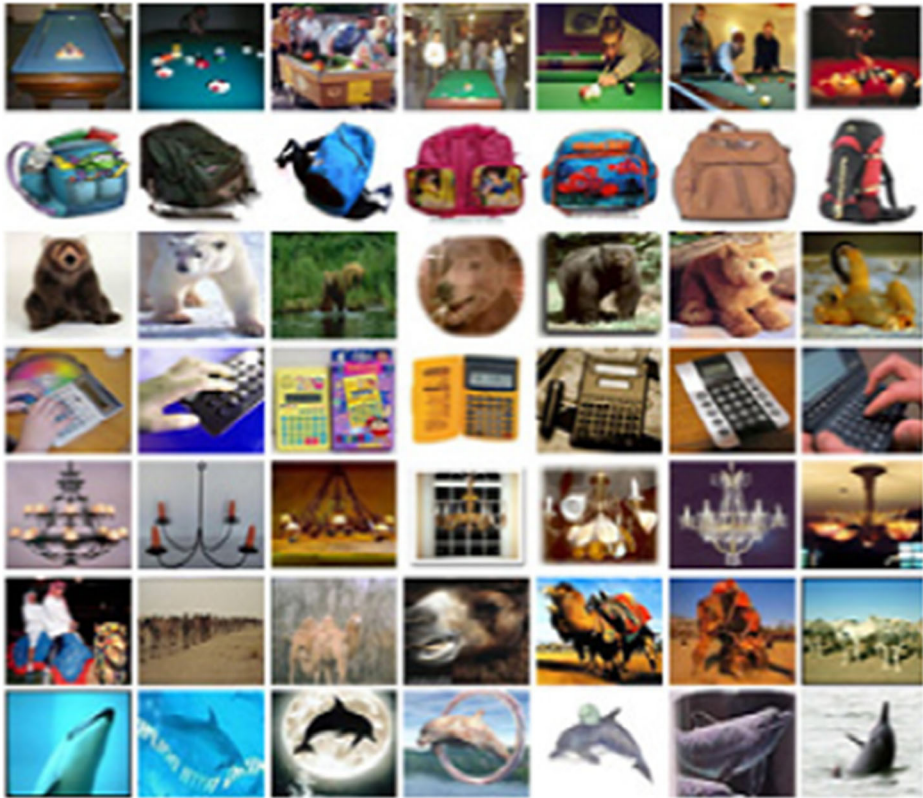


**Fig. 8** Collection of CALTECH-256 objects

effectiveness and the robustness of the proposed moments relative to other moments for three image database and for different classes.

### 6.3 Comparison of classification methods

In this section, we will compare our method of classification based on the shape descriptors which are invariant moments of CMMI with the classification method based on the descriptors based on Convolution Neural Network (CNN) [10], on Histograms of Oriented Gradient (HOG) [5] and on the Scale-Invariant Feature Transform (SIFT) [34].

The descriptors CNN is a hierarchical deep learning architecture. It is based on repeated convolutional operations which repeatedly filter the image at each stage. The filters are trainable, that is, they learn to adapt to the task at hand during learning.

The descriptors HOG is based on first order image gradients. The image gradients are pooled into overlapping orientation bins in a dense manner.

The descriptors SIFT is Based on first order gradients, it is evaluated around scale invariant feature points obtained using the difference of gaussian key point detector.

To assess the individual discriminant power of each of these characteristics, we have performed the tests of classification on two heterogeneous image databases COREL



Fig. 9 Collection of Corel objects

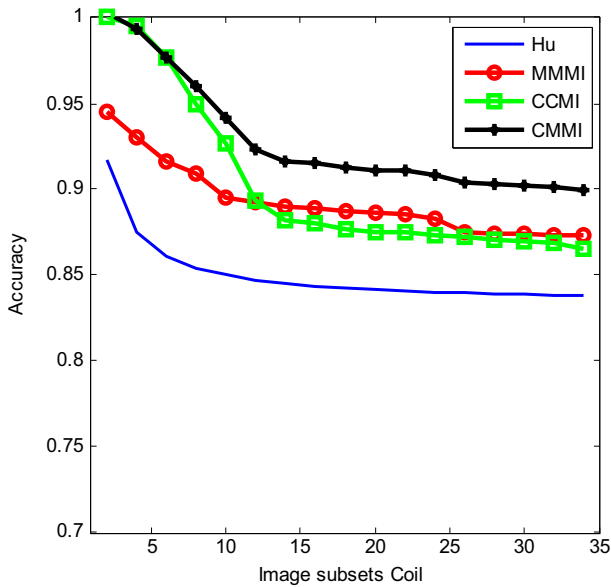
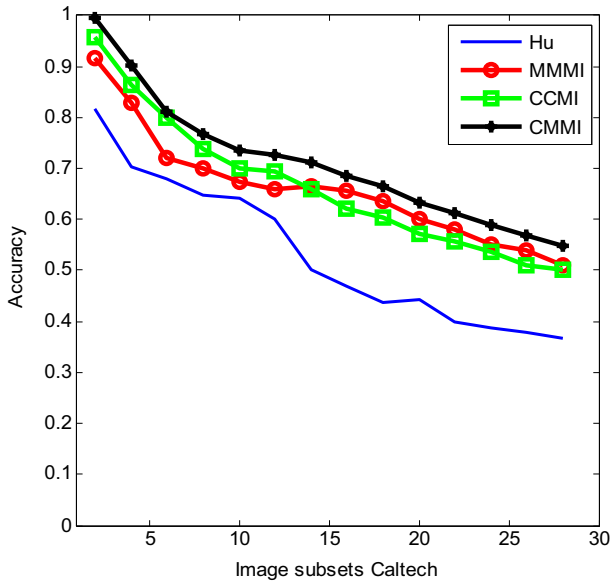


Fig. 10 Classification results of Columbia (COIL-100) database



**Fig. 11** Classification results of Caltech database

([http://www.vision.caltech.edu/Image\\_Datasets](http://www.vision.caltech.edu/Image_Datasets)) and CALTECH-256 (<http://wang.ist.psu.edu/docs/home.shtml>).

In this test, four sub-image databases, consisting respectively of 3, 7, 10 and 20 classes are used from the COREL database and the CALTECH-256 database. The performance of classification corresponding to each model, for the different sub databases used, are measured

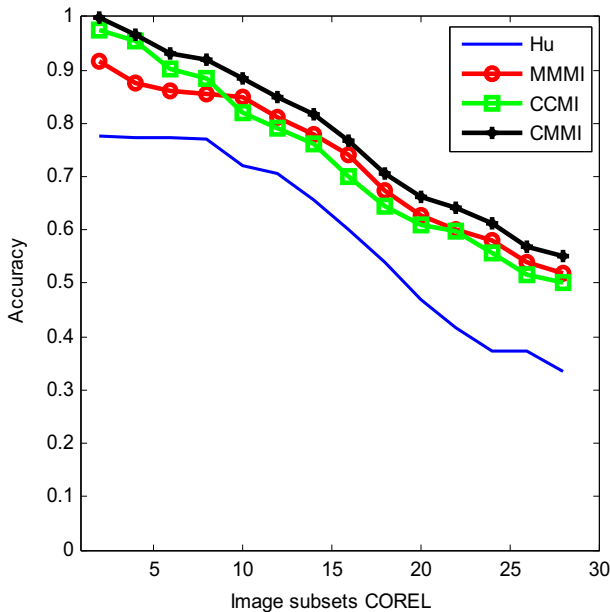


**Fig. 12** Classification results of Corel database

**Table 2** The classification rate of the sub-bases of COREL database by using the different features CNN, HOG, SIFT and CMMI

Image subsets	CNN	HOG	SIFT	CMMI
3 clusters set	0.9100	0.9250	0.9465	0.9620
7 clusters set	0.7060	0.7420	0.7532	0.8250
10 clusters set	0.6200	0.6400	0.6400	0.7600
20 clusters set	0.5500	0.5650	0.5800	0.6540

**Table 3** The classification rate of the sub-bases of CALTECH-256 database by using the different features CNN, HOG, SIFT and CMMI

Image subsets	CNN	HOG	SIFT	CMMI
3 clusters set	0.9200	0.9300	0.9465	0.9650
7 clusters set	0.6960	0.7020	0.7132	0.8425
10 clusters set	0.6300	0.6400	0.6500	0.7700
20 clusters set	0.5400	0.5550	0.5600	0.6450

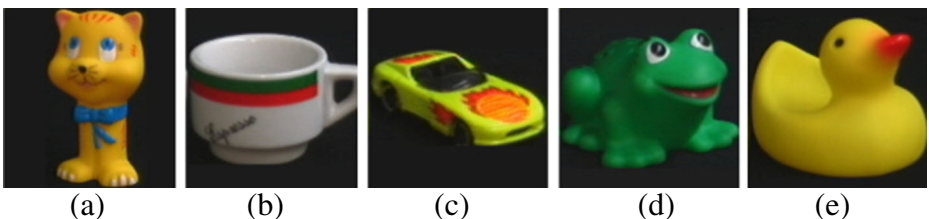
using simple classifiers based on Euclidean distances. Values of the accuracy of the recognition of assessed models for the four sub-bases of the COREL database and the CALTECH-256 are presented in Tables 2 and 3. The best and worst performances in these tables are shown in bold for the different sub-databases of the used images. The both Tables 2 and 3 show that the illustrated performances of classification well vary obviously depending on the different used characteristics. The performances of classification of a model of a given characteristic vary in terms of different sub-databases of the used images. This proves that the discriminating power of each feature is not absolute, but it varies considerably depending on the contents of the considered image.

According to Tables 2 and 3, the descriptors of the shape of CMMI is the most efficient among the various used CNN, HOG and SIFT for the classification of sub-bases of COREL and CALTECH-256 with 3, 7, 10 and 20 classes.

Finally we can see that among all the extracted features: CNN, HOG, SIFT and CMMI the descriptors of the shape of CMMI are often the most relevant that the descriptors of CNN, HOG and SIFT.

## 6.4 Computational time

In this sub-section, we will compare the computational time of Charlier-Meixner's invariant moments by two methods: the direct method described in sub-section 6.2

**Fig. 13** Set of test binary images **a** Car, **b** Ducke Box, **d** Cat and **e** Objet

**Table 4** Average times and reduction percentage for CMMI invariant moments of the five images

Image	Direct method	Proposed method	ETIR %
Cat	0,3678	0,1456	60,41%
Cup	0,3456	0,1335	61,37%
Car	0,3718	0,1546	58,42%
Frog	0,3775	0,1521	59,71%
Duck	0,3605	0,1496	58,50%

and the proposed fast method based on the image slice representation defined previously in section 6.3. For this, we will measure the computational time of the characteristic vector defined in equation Eq. (36) by two methods. To compare the two computational methods we will use the execution time improvement ratio (ETIR) as a criterion. This ratio is defined as  $ETIR = (1 - \text{Time1}/\text{Time2}) \times 100$ , where Time1 and Time2 are the execution time of the first and the second methods.  $ETIR = 0$  if both execution times are identical.

In the this experiment, a set of five gray-scale images with a size of  $128 \times 128$  pixels, shown in Fig. 13, selected from the Columbia Object Image Library (COIL-100) database [52] were used as test images. The computational processes are performed for each of the five images where the average times and execution-time improvement ratio (ETIR) are included in Table 4 for CMMI invariant moments using the proposed method described by the Eq. (28) and the direct method described by the Eq. (34). The result indicates again that our proposed method has a better performance than the direct method. Note that the algorithm was implemented on a PC Intel Core i5 2.40 GHz, 4GB of RAM.

The table shows that the proposed method is faster than the direct method and the saving of time reaches 60% because the computation of discrete orthogonal invariant moments CMMI proposed by the proposed method depends solely on the number of blocks and slices on the other hand the computation of the moments by the direct method depends on all the image.

## 7 Conclusion

In this paper, we have proposed a new method for the classification of the objects. This method is performed using a new set of discrete orthogonal moments of Charlier-Meixner and the image slice representation. Furthermore, we have derived a new set of Charlier-Meixner's invariant moments from the geometric invariant moments of each block in each slice of the image. Moreover, the accuracy of classification of the proposed CMMI in the classification of the object is carried out for three image databases. Hence, the classification results by our descriptor CMMI are better than that of Hu, CCMI and MMMI. In addition, our classification method is also better than other methods non-moments like the CNN, HOG and SIFT features. So, these moments have a desirable image representation capability and can be useful in the the recognition domain. In order to reduce the calculation cost of the Charlier-Meixner moments when classifying image databases which contains a large number of classes, we propose to study the reduction of the characteristic vector in the next work.

## References

1. Abu-Mostafa YS, Psaltis D (1984) Recognitive aspects of moment invariants. *IEEE Trans Pattern Anal Mach Intell* 6:698–706
2. Cheng D, Xianglong L, Yadong M (2015) Large-scale multi-task image labeling with adaptive relevance discovery and feature hashing. *Signal Process* 112:137–145
3. Chong C-W, Raveendran P, Mukundan R (2003) Translation invariants of Zernike moments. *Pattern Recogn* 36:1765–1773
4. Chong C-W, Raveendran P, Mukundan R (2004) Translation and scale invariants of Legendre moments. *Pattern Recogn* 37:119–129
5. Dalal N, Triggs B (2005) Histograms of oriented gradients for human detection. *Conf Comput Vis Pattern Recognit (CVPR'05)* 2:886–893
6. Dunkl CF, Xu Y (2001) Orthogonal polynomials of several variables. *Encyclopedia of mathematics and its applications*, vol 81. Cambridge University Press, Cambridge
7. Fernandez L, Perez TE, Perez MA (2007) Second order partial differential equations for gradients of orthogonal polynomials in two variables. *J Comput Appl Math* 199:113–121
8. Fernandez L, Prez TE, Pinar MA (2011) Orthogonal polynomials in two variables as solutions of higher order partial differential equations. *J Approx Theory* 163:84–97
9. Flusser J (2000) Refined moment calculation using image block representation. *Image Process IEEE Trans* 9(11):1977–1978
10. Garcia C, Delakis M (2004) Convolutional face finder: a neural architecture for fast and robust face detection. *IEEE Trans Pattern Anal Mach Intell* 26(11):1408–1423
11. Guyon I, Elisseeff A (2003) An introduction to variable and feature selection. *J Mach Learn Res* 3:1157–1182
12. Hmimid A, Sayyouri M, Qjidaa H (2014) Image classification using a new set of separable two-dimensional discrete orthogonal invariant moments. *J Electron Imaging* 23(1):013026
13. Hmimid A, Sayyouri M, Qjidaa H (2015) Fast computation of separable two-dimensional discrete invariant moments for image classification. *Pattern Recogn* 48(2):509–521
14. Hosny KM (2007) Exact and fast computation of geometric moments for gray level images. *Appl Math Comput* 189:1214–1222
15. Hosny KM (2011) Image representation using accurate orthogonal Gegenbauer moments. *Pattern Recogn Lett* 32:79s5–7804
16. Hu MK (1962) Visual pattern recognition by moment invariants. *IRE Trans Inf Theory* IT-8:179–187
17. Huijun H, Yuanxiang L, Maofu L (2014) Classification of defects in steel strip surface based on multiclass support vector machine. *Multimedia Tools Applic* 69(1):199–216
18. Huijun H, Ya L, Maofu L (2016) Surface defect classification in large-scale strip steel image collection via hybrid chromosome genetic algorithm. *Neurocomputing* 181:86–95
19. Jie X, Xianglong L, Zhouyuan H (2017) Multi-class support vector machine via maximizing multi-class margins”. In: *The 26th International Joint Conference on Artificial Intelligence (IJCAI 2017)*. <https://doi.org/10.24963/ijcai.2017/440>
20. Karakasis EG, Papakostas GA, Koulouriotis DE, Tourassis VD (2013) Generalized dual Hahn moment invariants. *Pattern Recogn* 46:1998–2014
21. Khotanzad A, Hong YH (1990) Invariant image recognition by Zernike moments. *IEEE Trans Pattern Anal Mach Intell* 12:489–497
22. Koekoek R, Lesky PA, Swarttouw RF (2010) Hypergeometric orthogonal polynomials and their q-analogues. Springer monographs in mathematics. Library of Congress control number: 2010923797
23. Koornwinder T (1975) Two-variable analogues of the classical orthogonal polynomials. *Theory and application of special functions*, proceedings of the advanced seminar Madison: University of Wisconsin Press, Academic Press, pp 435–495
24. Lei H, Xianglong L, Binqiang M (2015) Online semi-supervised annotation via proxy-based local consistency propagation. *Neurocomputing* 149:1573–1586
25. Liao SX, Pawlak M (1996) On image analysis by moments. *IEEE Trans Pattern Anal Mach Intell* 18(3): 254–266
26. Lim C, Honarvar B, Thung KH, Paramesran R (2011) Fast computation of exact Zernike moments using cascaded digital filters. *Inf Sci* 181:3638–3651
27. Liu Y, Nie L, Han L, Zhang L, Rosenblum DS (2015) Action 2 Activity: recognizing complex activities from sensor data. In: *IJCAI, Buenos Aires, Argentina*, pp 1617–1623
28. Liu Y, Nie L, Han L, Zhang L, Rosenblum DS (2016) From action to activity: sensor-based activity recognition. *Neurocomputing* 181:108–115
29. Liu L, Cheng L, Liu Y, Jia Y, Rosenblum DS (2016) Recognizing complex activities by a probabilistic interval-based model. *AAAI* 30:1266–1272

30. Liu Y, Zheng Y, Liang Y, Liu S, Rosenblum DS (2016) Urban water quality prediction based on multi-task multi-view learning
31. Liu Y, Zhang L, Nie L, Yan Y, Rosenblum DS (2016) Fortune teller: predicting your career path. In: AAAI, pp 201–207
32. Liu M, Zhang L, Hu H (2016) A classification model for semantic entailment recognition with feature combination. *Neurocomputing* 208:127–135
33. Liu M, JIAN L, Hu H (2017) Automatic extraction and visualization of semantic relations between medical entities from medicine instructions. *Multimedia Tools Applic* 76(8):10555–10573
34. Lowe D (2004) Distinctive image features from scale-invariant keypoints. *Int J Comput Vis* 60:91–110
35. Mukundan R, Ong SH, Lee PA (2000) Image analysis by Tchebichef moments. *IEEE Trans Image Process* 10(9):1357–1364
36. Nikiforov AF, Suslov SK, Uvarov B (1991) *Classical orthogonal polynomials of a discrete variable*. Springer, New York
37. Papakostas GA, Karakasis EG, Koulourisotis DE (2008) Efficient and accurate computation of geometric moments on gray-scale images. *Pattern Recogn* 41(6):1895–1904
38. Papakostas GA, Karakasis EG, Koulouriotis DE (March 2010) Accurate and speedy computation of image Legendre moments for computer vision applications. *Image Vis Comput* 28(3):414–423
39. D. Preoțiuc-Pietro, Y. Liu., D. Hopkins and L. Ungar, Beyond binary labels: political ideology prediction of twitter users. Proceedings of the 55th Annual Meeting of the Association for Computational Linguistics, vol. 1, pp 729–740, 2017
40. Sayyouri M, Hmimid A, Qjidaa H (2012) A fast computation of Charlier moments for binary and gray-scale images. In: *Information Science and Technology Colloquium (CIST)*. CIST, Fez, Morocco, pp 101–105, 22–24
41. Sayyouri M, Hmimid A, Qjidaa H (2012) A fast computation of hahn moments for binary and gray-scale images. In: *IEEE, International Conference on Complex Systems ICCS'12*, Agadir, pp. 1–6
42. Sayyouri M, Hmimid A, Qjidaa H (2012) A fast computation of Charlier moments for binary and gray-scale images. In: *The 2nd edition of the IEEE Colloquium on Information Sciences and Technology (CIST'12)*. CIST, Fez, Morocco
43. Sayyouri M, Hmimid A, Qjidaa H (2013) Improving the performance of image classification by Hahn moment invariants. *J Opt Soc Am A* 30:2381–2394
44. Sayyouri M, Hmimid A, Qjidaa H (2015) A fast computation of novel set of Meixner invariant moments for image analysis. *Circ Syst Signal Process Springer* 34(3):875–900
45. Shu HZ, Zhang H, Chen BJ, Haigron P, Luo LM (2010) Fast computation of Tchebichef moments for binary and gray-scale images. *IEEE Trans Image Process* 19(12):3171–3180
46. Spiliotis IM, Mertzios BG (1998) Real-time computation of two-dimensional moments on binary images using image block representation. *IEEE Trans Image Process* 7(11):1609–1615
47. Teague MR (1980) Image analysis via the general theory of moments. *J Opt Soc Amer* 70:920–930
48. Teh CH, Chin RT (1988) On image analysis by the method of moments. *IEEE Trans Pattern Anal Mach Intell* 10(4):496–513
49. Tsougenis ED, Papakostas GA, Koulouriotis DE (2014) Image watermarking via separable moments. *Multimedia Tools Applic*:1–28
50. Vapnik V (1999) An overview of statistical learning theory. *IEEE Trans Neural Netw* 10:988–999
51. Xu Y (2004) On discrete orthogonal polynomials of several variables. *Adv Appl Math* 33:615–663
52. Yap PT, Paramesran R, Ong SH (2003) Image analysis by Krawtchouk moments. *IEEE Trans Image Process* 12(11):1367–1377
53. Yingjie X, Luming Z, Zhenguang L (2017) Weakly supervised multimodal kernel for categorizing aerial photographs. *IEEE Trans Image Process* 26(8):3748–3758
54. Yonggang L, Ye Wei L, Liu J, Letian Z, Ye Liu S (2017) Towards unsupervised physical activity recognition using smartphone accelerometers. *Multimedia Tools and Applic* 76(8):10701–10719
55. Yuxing H, Liqiang N (2016) An aerial image recognition framework using discrimination and redundancy quality measure. *J Vis Commun Image Represent* 37:53–62
56. Zechao L, Jinhui T (2015) Weakly supervised deep metric learning for community-contributed image retrieval. *IEEE Trans Multimedia* 17(11):1989–1999
57. Zechao L, Jinhui T (2017) Weakly supervised deep matrix factorization for social image understanding. *IEEE Trans Image Process* 26(1):276–288
58. Zechao L, Jing L, Jinhui T (2015) Robust structured subspace learning for data representation. *IEEE Trans Pattern Anal Mach Intell* 37(10):2085–2098
59. Zhang H, Shu HZ, Haigron P, Li BS, Luo LM (2010) Construction of a complete set of orthogonal Fourier–Mellin moment invariants for pattern recognition applications. *Image Vis Comput* 28:38–44
60. Zhang L, Yang Y, Wang M (2016) Detecting densely distributed graph patterns for fine-grained image categorization. *IEEE Trans Image Process* 25(2):553–565

61. Zhu H (2012) Image representation using separable two-dimensional continuous and discrete orthogonal moments. *Pattern Recogn* 45(4):1540–1558
62. Zhu HQ, Shu HZ, Liang J, Luo LM, Coatrieux JL (2007) Image analysis by discrete orthogonal Racah moments. *Signal Process* 87(4):687–708
63. Zhu H, Shu H, Xia T, Luo L, Coatrieux JL (2007) Translation and scale invariants of Tehebichef moments. *Pattern Recogn* 40:2530–2542
64. Zhu H, Liu M, Shu H, Zhang H, Luo L (2010) General form for obtaining discrete orthogonal moments. *IET Image Process* 4(5):335–352



**Abdeslam Hmimid** received the B.Eng. degree in electrical engineering, with First Class Honors, and the M.S. degree in engineering science from the Faculty of science, University of Sidi Mohammed Ben Abdellah, Fez, Morocco in 2009 and 2011, respectively. He is currently pursuing the Ph.D. degree in the Department of physics, University of Sidi Mohammed Ben Abdellah, Fez, Morocco. His research interest includes image processing, pattern classification, orthogonal systems, and special functions.



**Mhamed Sayyouri** received the M.S. degree in engineering science and Ph.D degrees in Signals, Systems and Informatics from the Faculty of science, University of Sidi Mohammed Ben Abdellah, Fez, Morocco in 2002 and 2014, respectively. Since 2016, he served as a Research Scientist at the National School of Applied Sciences, Chouaib Doukkali University, Eljadida, Morocco. He has been a Professor with the Department of Department of Industrial Sciences and Technologies (STIN). His research interest includes image processing, pattern classification Signals and Systems.





**Hassan Qjidaa** received the M.S. and Ph.D. degrees in electrical engineering from Nuclear Physics Institute of Lyon, in France 1984 and 1987, respectively. Since 1987, he served as a Research Scientist at Faculty of science in the University of Sidi Mohammed Ben Abdellah, Fez, Morocco. He has been a Professor with the Department of Physics. He is currently also a Director of the Information Analysis and Micro-system Teams (IAMS), and Vice Director of the electronic signal and systems laboratory (LESSI). His current research interests are in image processing, pattern recognition, data analysis and machine intelligence.